Fig.Supporting Information

Tailorable Nanoarchitecturing of Bimetallic Nickel-Cobalt Hydrogen Phosphate via the Self-Weaving of Nanotubes for Efficient Oxygen Evolution

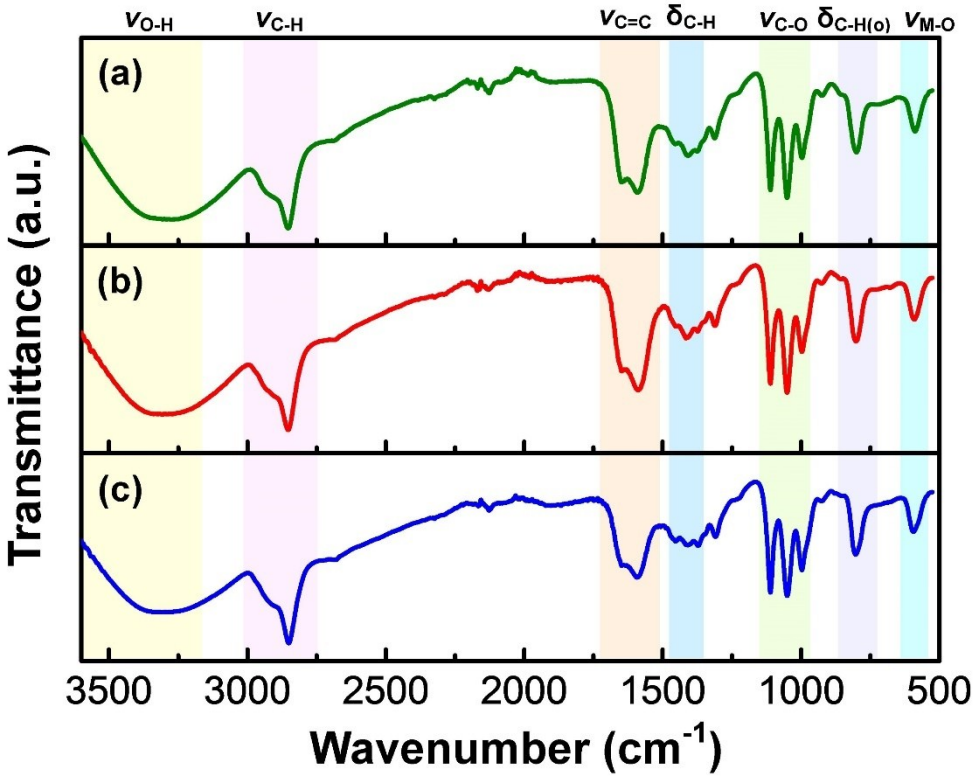

Fig. S1. Enlarged FTIR spectra of (a) NiCo-0.5 glycerate, (b) NiCo-1.0 glycerate, and (c) NiCo-2.0 glycerate with detailed assignments.

Table S1. The molar ratios of Ni, Co, and P for each bimetallic Ni-Co hydrogen phosphate samples based on ICP measurements

Sample	H_3PO_4 amount (μL)	*n* (Ni/Co)	*n* (Co/Co)	*n* (P/Co)
NiCo-2.0-200HP	200	2	1.02	3.62
NiCo-2.0-300HP	300	2	1.08	4.62
NiCo-2.0-500HP	500	2	1.04	4.78
NiCo-2.0-800HP	800	2	1.06	5.06
NiCo-1.0-200HP	200	1	1.03	3.18
NiCo-1.0-300HP	300	1	1.20	3.81
NiCo-1.0-500HP	500	1	1.24	3.92
NiCo-1.0-800HP	800	1	1.10	5.82
NiCo-0.5-200HP	200	1	2.19	3.24
NiCo-0.5-300HP	300	1	2.71	3.30
NiCo-0.5-500HP	500	1	2.01	3.46
NiCo-0.5-800HP	800	1	2.15	2.96

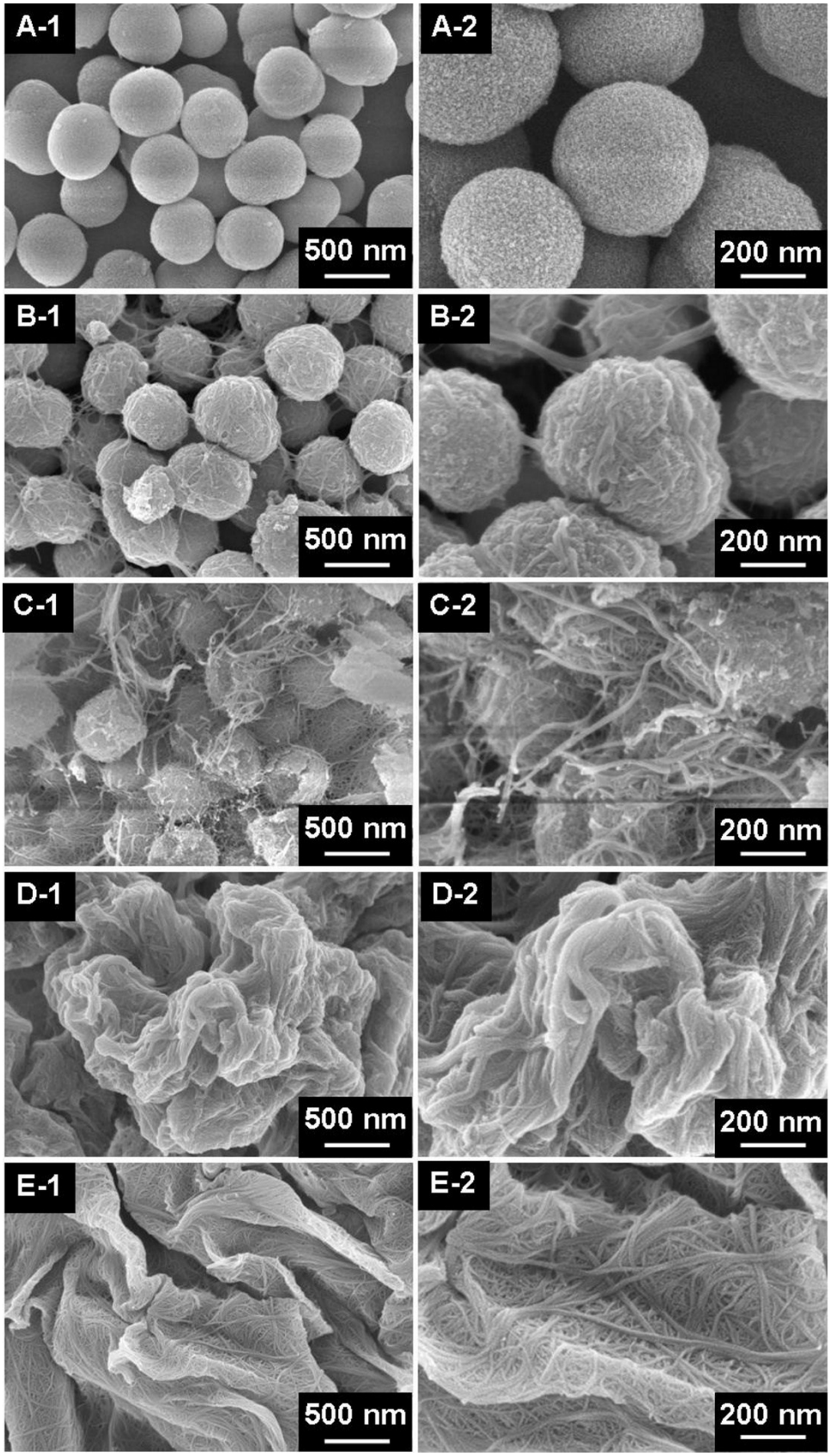

Fig. S2. SEM images showing the morphological evolutions of NiCo-2.0 glycerate spheres (A-1, A-2) after the solvothermal reactions with 200 μL (B-1, B-2), 300 μL (C-1, C-2), 500 μL (D-1, D-2), and 800 μL (E-1, E-2) of H_3PO_4 solution in ethanol at 180 °C for 16 h.

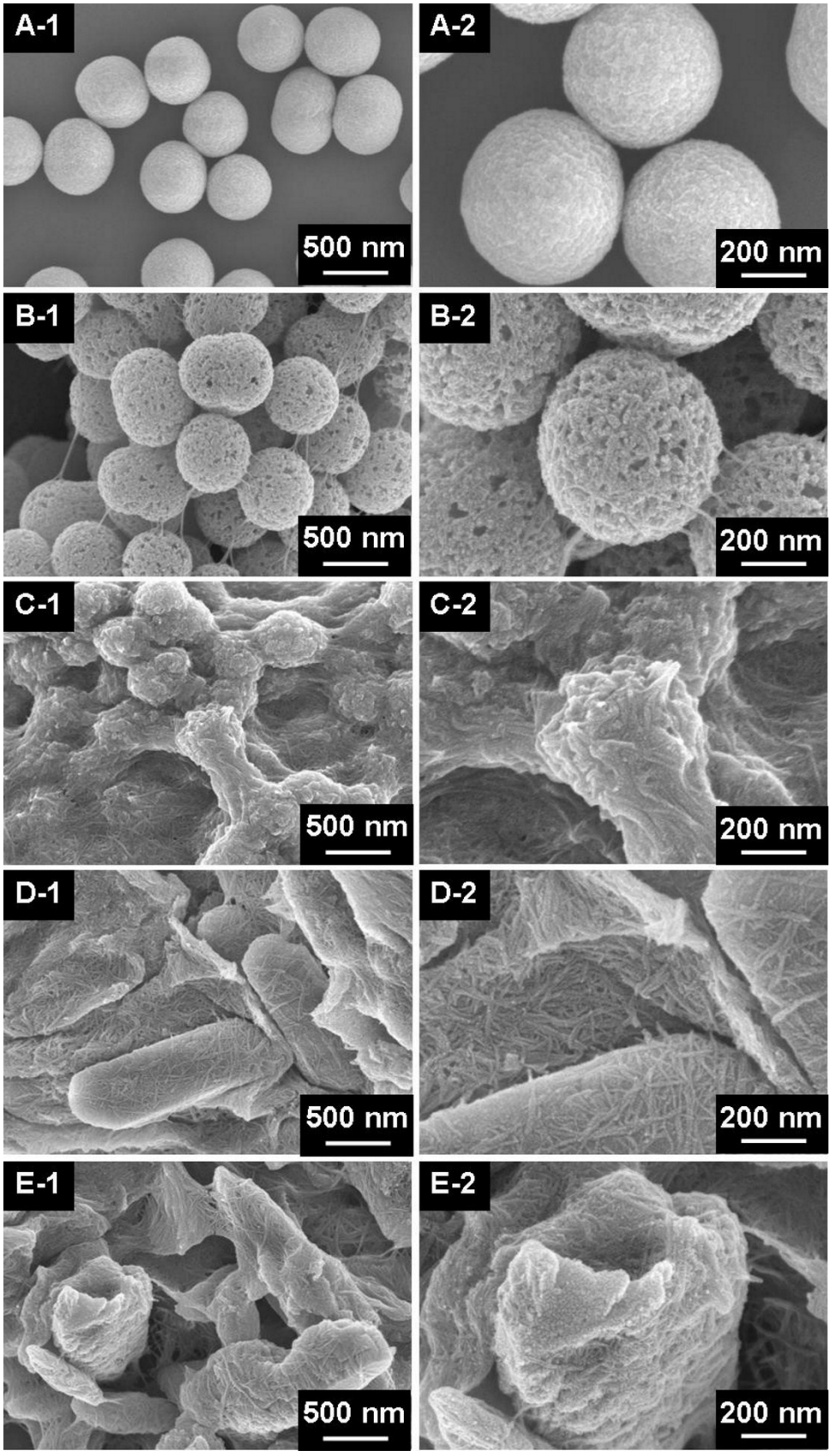

Fig. S3. SEM images showing the morphological evolutions of NiCo-1.0 glycerate spheres (A-1, A-2) after the solvothermal reactions with 200 μL (B-1, B-2), 300 μL (C-1, C-2), 500 μL (D-1, D-2), and 800 μL (E-1, E-2) of H_3PO_4 solution in ethanol at 180 °C for 16 h.

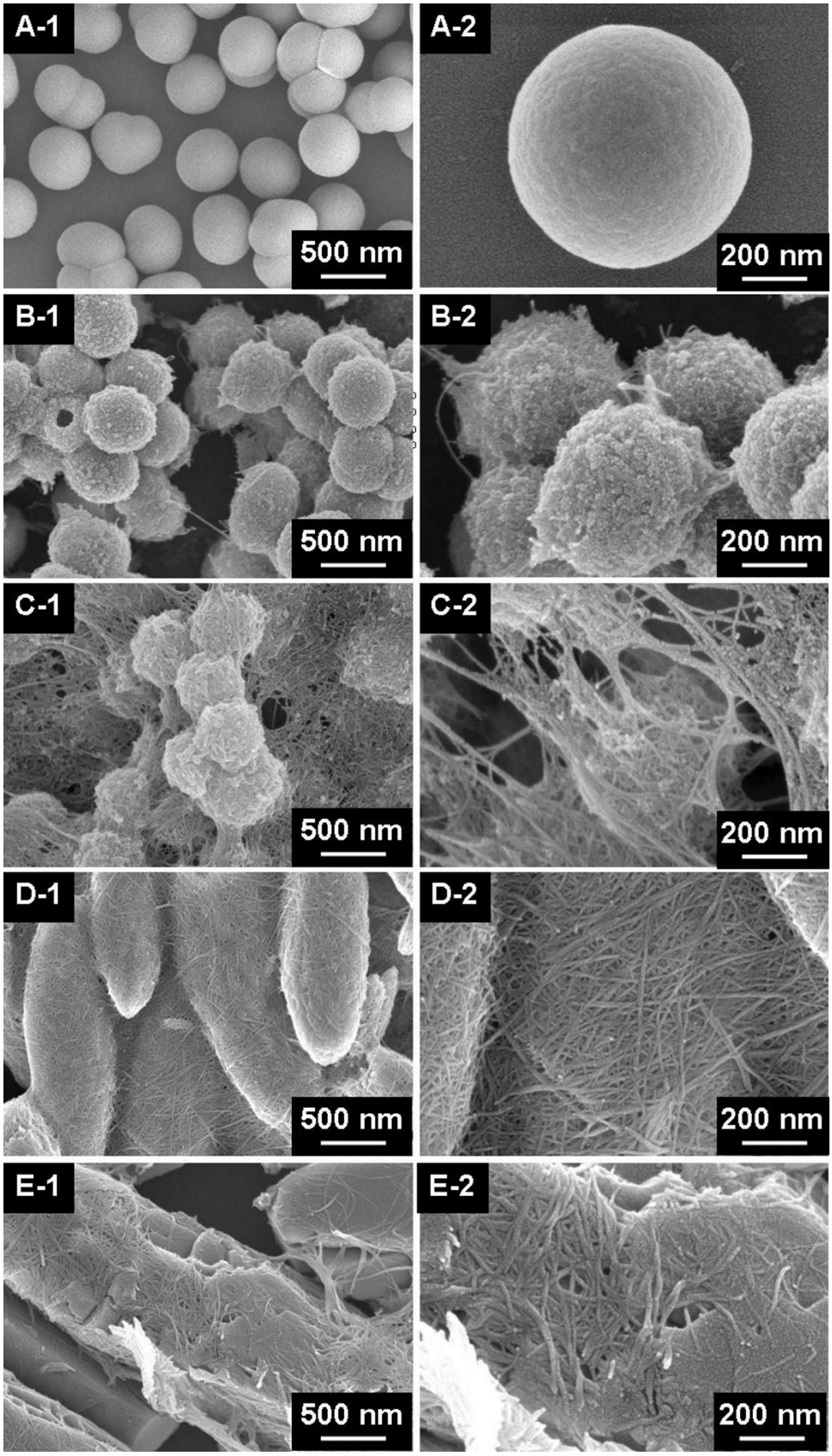

Fig. S4. SEM images showing the morphological evolutions of NiCo-0.5 glycerate spheres (A-1, A-2) after the solvothermal reactions with 200 μL (B-1, B-2), 300 μL (C-1, C-2), 500 μL (D-1, D-2), and 800 μL (E-1, E-2) of H_3PO_4 solution in ethanol at 180 °C for 16 h.

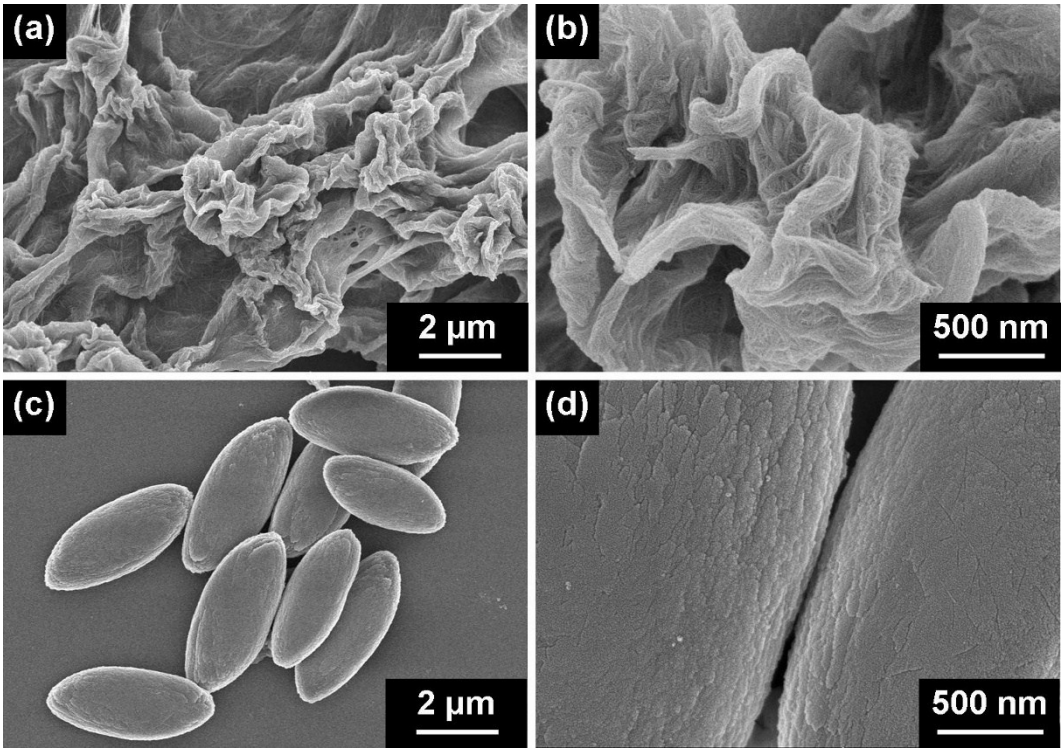

Fig. S5. Low- and high-magnification SEM images of nickel (a, b) and cobalt (c, d) hydrogen phosphate prepared by solvothermal reactions with 800 μL of phosphoric acid (H_3PO_4) at 180 °C for 16 h using nickel glycerate and cobalt glycerate, respectively as sacrificial templates.

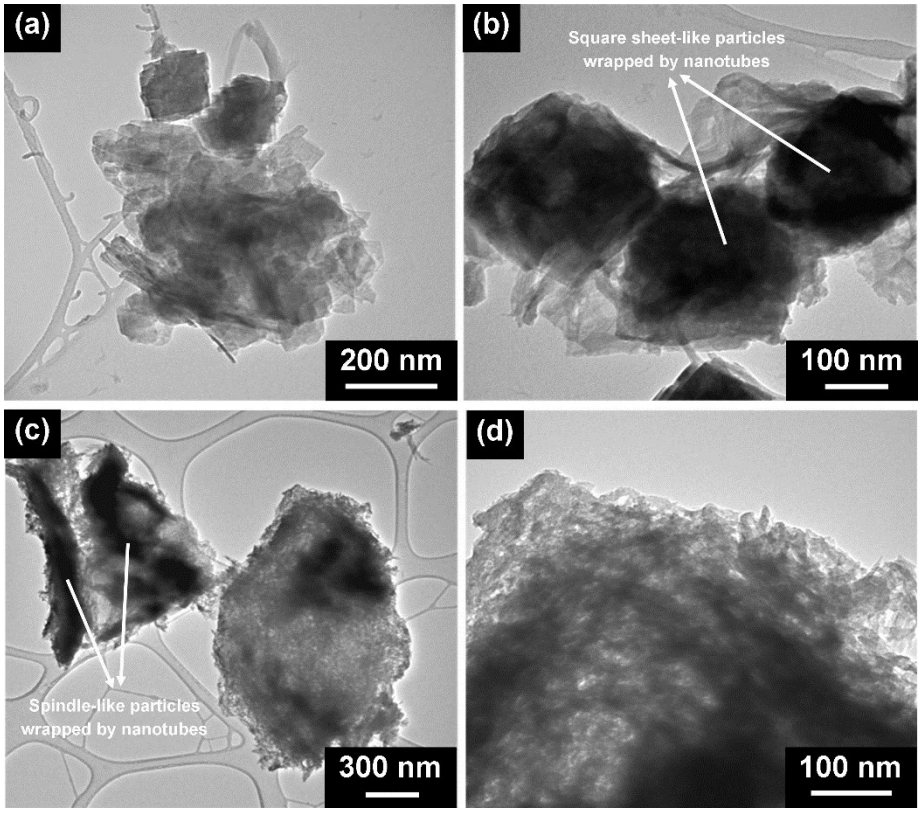

Fig. S6. TEM images of NiCo-1.0-800HP (a, b), and NiCo-0.5-800HP (c, d)

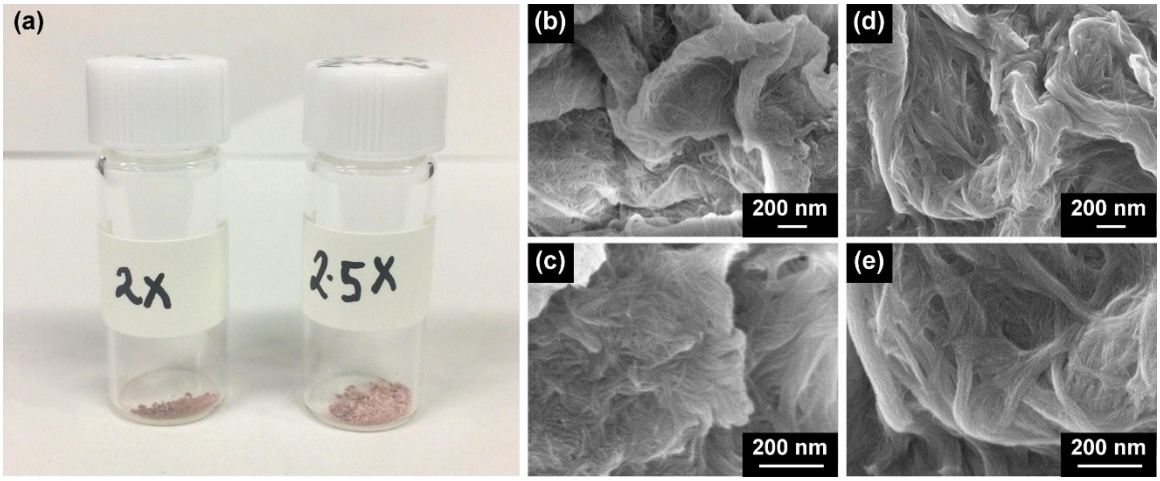

Fig. S7. (a) Digital photographs of the Ni-Co hydrogen phosphate products obtained with the same procedures used for synthesizing NiCo-2.0-800HP but by increasing the amounts of all reactants by 2 times (*left*: NiCo-2.0-800HP-2x) and 2.5 times (*right*: NiCo-2.0-800HP-2.5x). Low- and high-magnification images of NiCo-2.0-800HP-2x (b, c) and NiCo-2.0-800HP-2.5x (d, e). The Ni/Co ratio was maintained at 2:1 in both cases.

The potential for large-scale preparation was explored by increasing the amounts of reagents (including the NiCo-2.0 glycerate template, H_3PO_4 and ethanol) used in the synthesis of NiCo-2.0-800HP by 2 times and 2.5 times (**Fig. S7a**). When the amount of the NiCo-2.0 glycerate template used during the synthesis of NiCo-2.0-800HP was increased to 60 mg and 75 mg (while also increasing the amounts of H_3PO_4 and ethanol), approximately 28 mg and 47.5 mg of Ni-Co hydrogen phosphate powders were obtained, respectively. This indicates that the yield is around 45-60%, taking into account that some products were lost during washing. Therefore, if we assume the yield is 50%, approximately 200 mg and 2 g of the Ni-Co glycerate template is needed to obtain 100 mg and 1 g of Ni-Co hydrogen phosphate product, respectively. Most importantly, the nanotube-assembled 2D architectures were successfully maintained during the scale-up preparation, as seen in **Fig. S7b-e**.

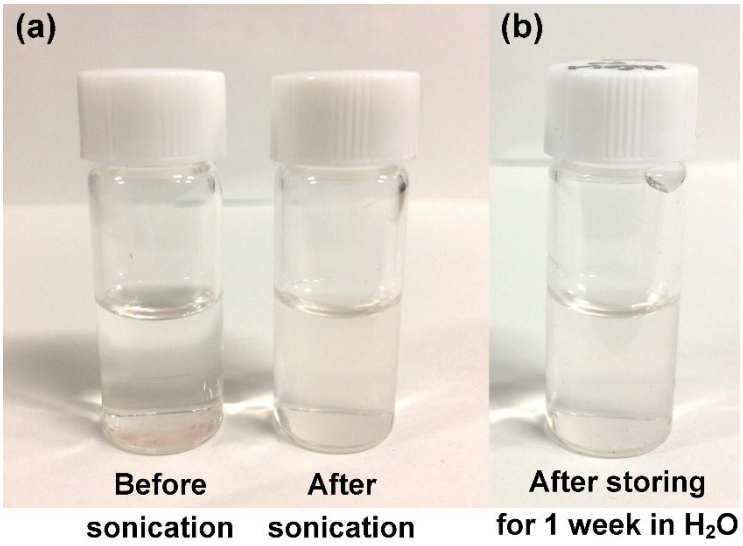

Fig. S8. (a) Digital photographs of NiCo-2.0-800HP in water before (left) and after sonication (right) and (b) after storing in H_2O for 1 week (without sonication or shaking), highlighting the excellent dispersability of this sample in H_2O.

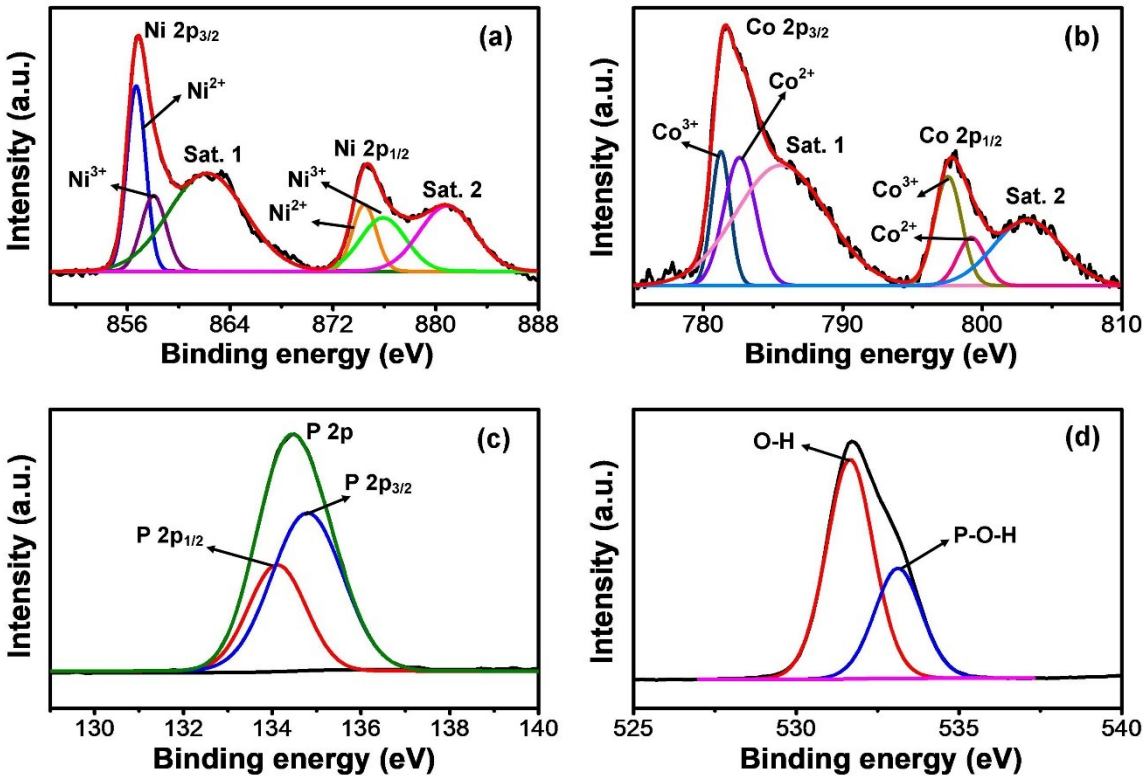

Fig. S9. High-resolution XPS spectra for Ni 2p (a), Co 2p (b), P 2p (c) and (d) O 1s of NiCo-2.0-800HP.

Table S2. Comparison of the OER activity of the fabricated NiCo-2.0-800HP electrode with transition metal phosphate-based electrodes reported in the literature

Electrode	Electrolyte	η_{10} (mV)	Tafel slope (mV dec^{-1})	Reference
Nanotube-woven Ni-Co hydrogen phosphate sheet-like (NiCo-2.0-800HP)	1.0 M KOH	320	84.0	This work
Cobalt phosphate nanoarray	0.1 M PBS	450	N/A	[1]
Graphene foam-supported cobalt phosphate	0.1 M K KPi	390	68.0	[2]
Carbon nanodots-modified cobalt phosphate	0.1 M KOH	350	59.0	[3]
3D CoFePi network	0.1 M KOH	315	33.0	[4]
Hollow cobalt phosphate spheres	1.0 M KOH	320	85.0	[5]
Co^{3+}-rich $Na_{1.95}CoP_2O_7$ phosphate	0.1 M KOH	390	44.0	[6]
$NaCo(PO_3)_3$ with partially graphitized carbon	1.0 M KOH	340	76.0	[7]
Cobalt pyrophosphate ($Co_2P_2O_7$) nanowires	1.0 M KOH	359	54.1	[8]
Cobalt pyrophosphate ($Co_2P_2O_7$) nanobelts	1.0 M KOH	371	57.9	[8]
Cobalt pyrophosphate ($Co_2P_2O_7$) nanoleaves	1.0 M KOH	390	81.6	[8]
Cobalt pyrophosphate ($Co_2P_2O_7$) nanorhombuses	1.0 M KOH	424	119	[8]
$Co_2P_2O_7$@C nanocrystals	0.1 M KOH	397	70.0	[9]
CoP_2O_7 nanocrystals	0.1 M KOH	490	86.0	[9]
$Co_3(PO_4)_2$@N-doped carbon	1.0 M KOH	317	62.0	[10]
Flower-like Co-Zn phosphate	1.0 M KOH	382	83.2	[11]
FeCo phosphate nanosheets	1.0 M KOH	267	30.0	[12]
$Co_3(PO_4)_2$@N-doped carbon	1.0 M KOH	290	82.0	[13]

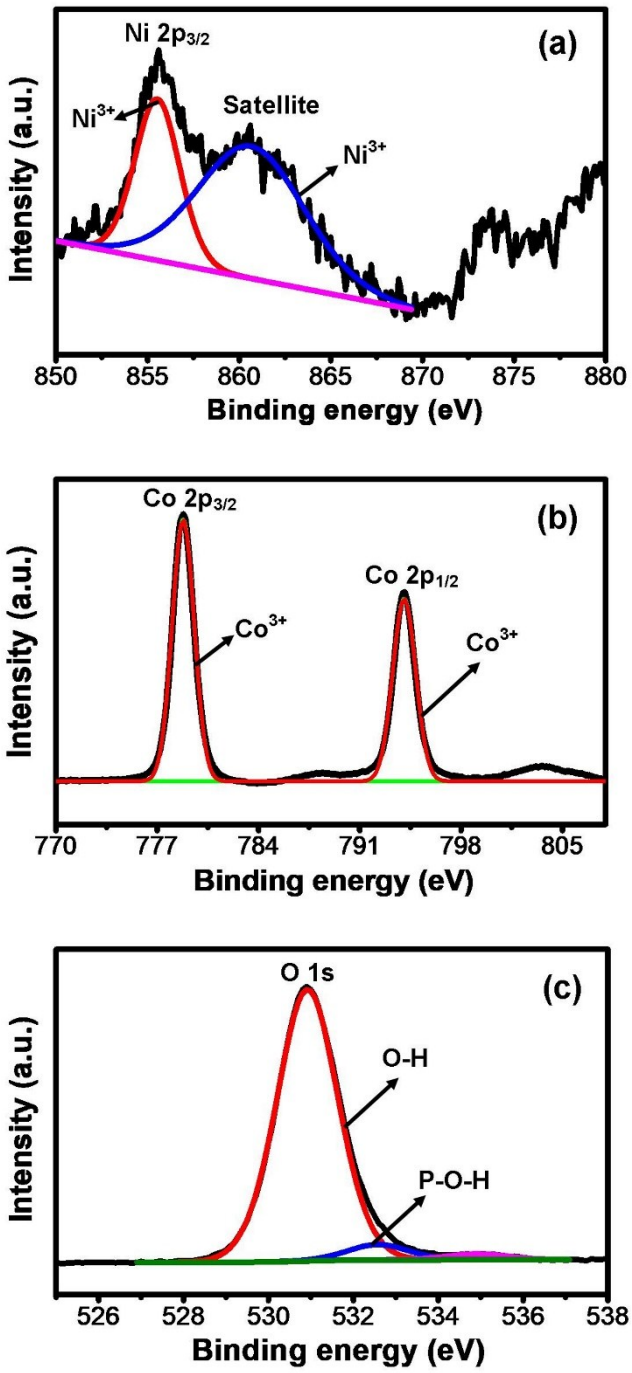

Fig. S10. High-resolution XPS spectra for (a) Ni 2p, (b) Co 2p, and (c) O 1s of the NiCo-2.0-800HP electrode after the OER stability test in 1.0 M KOH for 15 h.

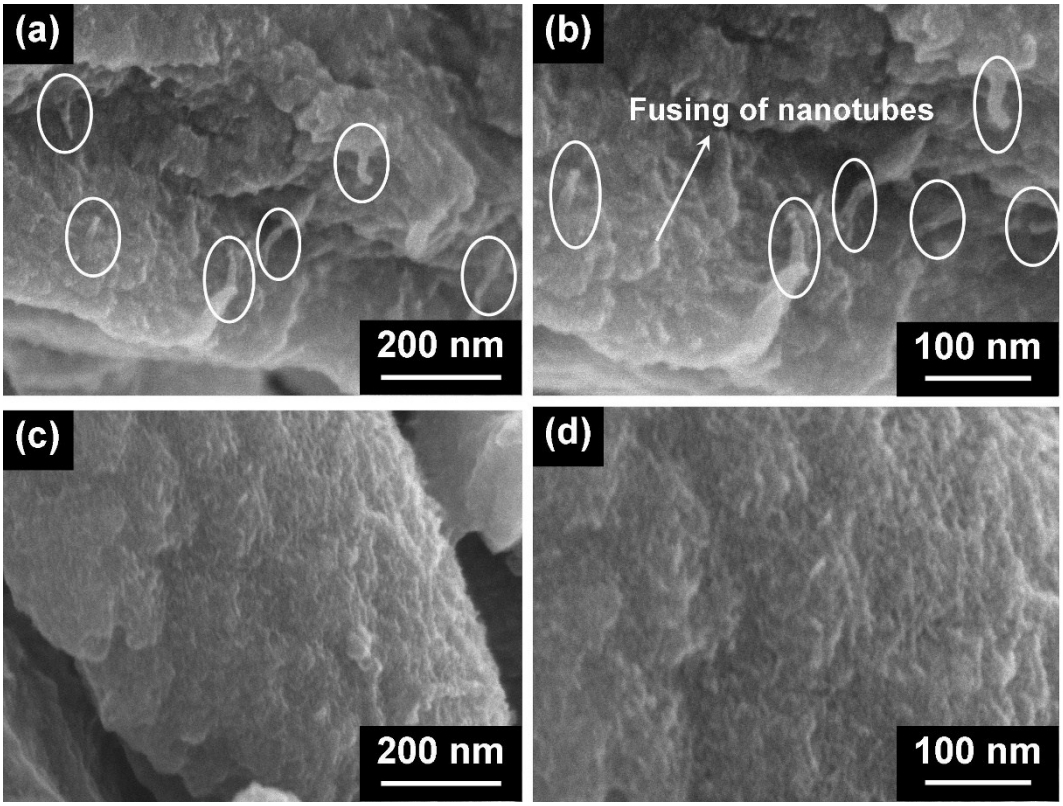

Fig. S11. Low- and high-magnification SEM images of NiCo-2.0-800HP after cycling (a, b) and NiCo-1.0-800HP after the OER catalytic reaction (c, d).

SI References

1. L. Xie, R. Zhang, L. Cui, D. Liu, S. Hao, Y. Ma, G. Du, A. M. Asiri and X. Sun, *Angew. Chem. Int. Ed.*, 2017, **56**, 1064-1068.
2. M. Zeng, H. Wang, C. Zhao, J. Wei, W. Wang and X. Bai, *Sci. Bull.*, 2015, **60**, 1426-1433.
3. S. Zhao, C. Li, H. Huang, Y. Liu and Z. Kang, *J. Materiomics*, 2015, **1**, 236-244.
4. Y. Zhou and H. C. Zeng, *Small*, 2018, **14**, 1704403.
5. L. Chen, J.-T. Ren, Y.-S. Wang, W.-W. Tian, L.-J. Gao and Z.-Y. Yuan, *ACS Sustain. Chem. Eng.*, 2019, **7**, 13559-13568.
6. L. Gui, X. Miao, C. Lei, K. Wang, W. Zhou, B. He, Q. Wang and L. Zhao, *Chem.-Euro J.*, 2019, **25**, 11007-11014.
7. R. Gond, D. K. Singh, M. Eswaramoorthy and P. Barpanda, *Angew. Chem. Int. Ed.*, 2019, **58**, 8330-8335.
8. H. Du, W. Ai, Z. L. Zhao, Y. Chen, X. Xu, C. Zou, L. Wu, L. Su, K. Nan, T. Yu and C. M. Li, *Small*, 2018, **14**, 1801068.
9. Y. Chang, N.-E. Shi, S. Zhao, D. Xu, C. Liu, Y.-J. Tang, Z. Dai, Y.-Q. Lan, M. Han and J. Bao, *ACS Appl. Mater. Interfaces*, 2016, **8**, 22534-22544.
10. C.-Z. Yuan, Y.-F. Jiang, Z. Wang, X. Xie, Z.-K. Yang, A. B. Yousaf and A.-W. Xu, *J. Mater. Chem. A*, 2016, **4**, 8155-8160.
11. L. Qian and Y. Miao, *Polyhedron*, 2019, **160**, 213-218.
12. D. Yin, Z. Jin, M. Liu, T. Gao, H. Yuan and D. Xiao, *Electrochem. Acta*, 2018, **260**, 420-429.
13. P. Feng, X. Cheng, J. Li and X. Luo, *Catal. Lett.*, 2018, **148**, 214-219.